Inorganic Chemistry

Article

pubs.acs.org/IC

Ruthenium Complexes of Thiaporphyrin and Dithiaporphyrin

Chuan-Hung Chuang,[†,§] Chen-Kuo Ou,[‡] Shan-Tung Liu,[†] Anil Kumar,[†,⊥] Wei-Min Ching,[†,∥] Pei-Chun Chiang,[†] Mira Anne C. dela Rosa,[†] and Chen-Hsiung Hung*[,†]

[†]Institute of Chemistry, Academia Sinica, Nankang, Taipei 115, Taiwan

[‡]Department of Chemistry, National Changhua University of Education, Changhua 500, Taiwan

[§]Department of Chemistry, National Tsing Hua University, Hsinchu 300, Taiwan

[∥]Department of Chemistry, National Taiwan Normal University, Taipei 106, Taiwan

Supporting Information

ABSTRACT: Successful synthesis and characterization of the six-coordinated complex [Ru(STTP)(CO)Cl] (**1**; STTP = 5,10,15,20-tetratolyl-21-thiaporphyrinato) allowed the development of the coordination chemistry of ruthenium−thiaporphyrin through dechlorination and metathesis reactions. Accordingly, [Ru^{II}(STTP)(CO)X] (X = NO_3^- (**2**), NO_2^- (**3**), and N_3^- (**4**)) was synthesized and analyzed by single-crystal X-ray structural determination and NMR, UV−vis, and FT-IR spectroscopic methods. An independent reaction of STPPH and [Ru(COD)Cl_2] led to [Ru^{III}(STTP)Cl_2] (**5**), which possessed a higher-valent Ru(III) center and exhibited good stability in the solution state. This stability allowed reversible redox processes in a cyclic voltammetric study. Reactions of [Ru(S_2TTP)Cl_2] (S_2TTP = 5,10,15,20-tetratolyl-21,23-dithiaporphyrinato) with $AgNO_3$ and NaSePh, also via the metathesis strategy, resulted in novel dithiaporphyrin complexes [Ru^{II}(S_2TTP)$(NO_3)_2$] (**6**) and [Ru^0(S_2TTP)$(PhSeCH_2SePh)_2$] (**7**), respectively. The structures of **6** and **7** were corroborated by X-ray crystallographic analyses. Complex **7** is an unprecedented ruthenium(0)−dithiaporphyrin with two *bis*(phenylseleno)methanes as axial ligands. A comparison of the analyses of the crude products from reactions of NaSePh and CH_2Cl_2 with or without [Ru(S_2TTP)Cl_2], further supported by UV−vis spectral changes under stoichiometric reactions between [Ru(S_2TTP)Cl_2] and NaSePh, suggested a reaction sequence in the order of (1) formation of a putative [Ru^{II}(S_2TTP)$(SePh)_2$] intermediate, followed by (2) the concerted formation of PhSe−CH_2Cl and simultaneously a reduction of Ru(II) to Ru(0) and finally (3) nucleophilic substitution of $PhSeCH_2Cl$ by excess $PhSe^-$, resulting in $PhSeCH_2SePh$, which readily coordinated to the Ru(0) and completed the formation of *bis*(phenylseleno)methane complex **7**.

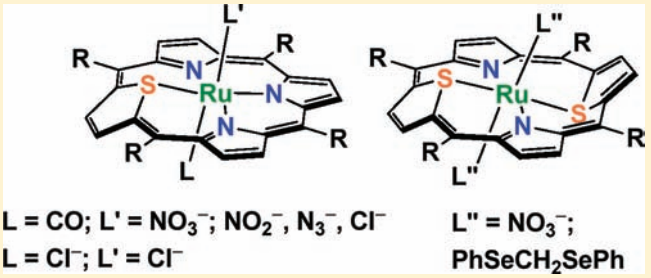

INTRODUCTION

Metalloporphyrins have been extensively used as catalysts to study biomimetic oxidation reactions.[1−4] Although not as broadly examined as metal complexes of regular porphyrin, core-modified porphyrins, e.g., carbon-,[5,6] silicon-,[7] phosphorus-,[8] and chalcogen-containing porphyrins,[9,10] which exhibit distinctively different chemical properties from regular porphyrins, have the potential to catalytically functionalize hydrocarbon substrates.

Bioinspired catalytic reactions using metalloporphyrins as catalysts can be performed not only by iron porphyrins but also by chromium,[11,12] manganese,[13,14] and ruthenium analogues. Ruthenium porphyrins containing a wide variety of peripheral substituents under different metal oxidation states have been reported to exhibit high activity toward catalytic reactions. As an example, dioxo(tetramesitylporphyrinato)ruthenium(VI), first reported by Groves and co-workers, showed good activity for the aerobic epoxidation of olefins.[15] Density function theory (DFT) calculations revealed that the low-spin ruthenium−oxo species, which are more electrophilic and robust catalysts than iron−oxo counterparts, gave lower hydrogen abstraction barriers toward a concerted hydroxylation mechanism.[16] Additionally, conversion of cyclohexene to 2-cyclohexen-1-ol through an aerobic oxidation at room temperature has been successfully achieved using perhalogenated ruthenium complex [(TFPPCl_8)Ru(CO)] (TFPPCl_8 = octachloro[tetrakis(pentafluorophenyl)]porphyrin) as the catalyst.[15] Recently, hydroxylation of hydrocarbons utilizing ruthenium(II)−carbonyl tetrakis(pentafluorophenyl)porphyrin complex [Ru^{II}(TPFPP)(CO)], in the presence of 2,6-dichloropyridine *N*-oxide as an oxidant, displayed good yields and high turnover numbers.[17] On the contrary, the development of ruthenium core-modified porphyrin chemistry is lagging far behind. Even though structurally characterized metal complexes of Ni(II),[18−20] Hg(II),[21] Pd(II),[22] Fe(II),[18] Cu(II),[9,18] Rh(III),[23] and Li(I) with a core-modified porphyrin as the ligand have been documented, there is no report on the preparation of the ruthenium−thiaporphyrin complex.[24] It was not until recently that metal−dithiaporphyrin complex [Ru^{II}(S_2TTP)Cl_2] was

Received: May 10, 2011
Published: November 7, 2011

synthesized and structurally characterized.[25] Because the presence of long carbon−sulfur and metal−sulfur bonds in the thiaporphyrin complexes resulted in a distorted porphyrin core, the stability of thiaporphyrin complexes was significantly decreased. Consequently, spontaneous demetalation of Fe(II)−tetraphenyl-21-thiaporphyrin in the solution state has been observed.[18] Interestingly, [$Ru^{II}(S_2TTP)Cl_2$] exhibited reversible redox processes under cyclic voltammetric measurements, which demonstrates good stability of this complex in the solution state.[25] To gain more insight into the ruthenium chemistry of sulfur-containing core-modified porphyrins, herein we reported the syntheses, characterizations, and crystal structures of new ruthenium−thiaporphyrin and dithiaporphyrin complexes.

EXPERIMENTAL SECTION

Instruments. Schlenk techniques and a nitrogen atmospheric drybox (Innovative Technology, Inc.) were used for handling air-sensitive compounds. UV−vis spectra were recorded on an Agilent HP8453 spectrophotometer. Elemental analyses (C, H, N) were obtained on a CHN analyzer (Heraeus). ^{1}H and ^{13}C NMR spectra were measured on a Varian Unity Inova Bruker AMX 400 or a Bruker AC 200 spectrometer. Chemical shifts are expressed in parts per million relative to residual $CHCl_3$ (7.258 ppm). Infrared spectra were recorded on a Biorad FTS-185 spectrophotometer. All cyclic voltammetric experiments were performed with a CHI 600D Potentiostat/Galvanostat (CH Instruments, Inc.). The cell consisted of a glassy carbon working electrode, a platinum wire auxiliary electrode, and a silver wire reference electrode, with 0.1 M tetra-*n*-butylammonium hexafluorophosphate as the supporting electrolyte in THF.

Materials. Dichloromethane and chloroform were dried with calcium hydride and distilled under nitrogen. Toluene and hexane were distilled under nitrogen in the presence of sodium chips using benzophenone ketyl as an indicator. Dried solvents, which were transferred into round-bottom flasks, bubbled with nitrogen for at least 10 min to remove residual dioxygen, and then sealed with a J-Young cap, were stored in the nitrogen atmosphere drybox prior to use. Pyrrole was freshly distilled under nitrogen from calcium hydride prior to use. Other starting materials were obtained commercially and used directly without further purification. Silica gel (100−120 mesh, Merck) or neutral alumina (Merck) was used for column chromatography. The starting 5,10,15,20-tetra-*p*-tolyl-21-thiaporphyrin, STTPH, was prepared using a mixed condensation of 2,5-bis-(tolylhydroxylmethyl)-thiophene, pyrrole, and *p*-tolylaldehyde or a condensation of 2,5-bis-(tolylhydroxylmethyl)thiophene and 5-*p*-tolyl-dipyrromethane according to the literature method.[24] 5,10,15,20-Tetra-*p*-tolyl-21,23-dithiaporphyrin, S_2TTP, was prepared through a condensation of 2,5-bis-(tolylhydroxylmethyl)thiophene and pyrrole.[25] Sodium phenylselenide was prepared from the reaction of diphenyl diselenide with sodium chips in anhydrous THF.

Preparation of [Ru(STTP)(CO)Cl] (1). In a Schlenk flask, the solution of STTPH (0.2 g, 0.291 mmol) and $Ru_3(CO)_{12}$ (0.4 g, 0.625 mmol) in *o*-dichlorobenzene (100 mL) was degassed with N_2. The solution was heated to reflux for 2.5 h under N_2. The completion of the reaction was confirmed from the absence of $STTPH_3^{2+}$ absorption in UV−vis spectra after the addition of TFA into the aliquots solution diluted in CH_2Cl_2. The reaction mixture was then cooled to room temperature and passed through a sinter-glass filter filled with Celite. The brown filtrate was combined and dried using a rotovap to give a black solid. The crude solid was then dissolved in 100 mL of CH_2Cl_2 and washed with 0.1 M HCl(aq). The CH_2Cl_2 solution was dried over $MgSO_4$, and the solvent was evaporated in vacuo to give a black solid. The crude product was recrystallized from dichloromethane/*n*-hexane to afford black solid **1**. Yield: 0.10 g (40%). ^{1}H NMR (200 MHz, 25 °C, chloroform-*d*, ppm): 9.26 (s, 2H, *β*-thiophene-H), 8.66 (d, *J* = 5.2 Hz, 2H, *β*-pyrrole-H), 8.61 (d, *J* = 5.1 Hz, 2H, *β*-pyrrole-H), 8.57 (s, 2H, *β*-pyrrole -H), 8.06 (m, 4H, tolyl-H), 7.73 (d, *J* = 8.0 Hz, 2H, tolyl-H), 7.50 (m, 10H, tolyl-H), 2.67 (s, 12H, *p*-tolyl-CH_3). UV−vis in CH_2Cl_2 [λ_{max}, nm, (log ε)]: 433 (4.64), 575 (3.64), 690 (3.50). Infrared (KBr, cm^{-1}): $\nu_{(CO)}$ = 1956. Elemental Anal. Calcd. (found) for $Ru_1C_{49}H_{36}N_3S_1O_1Cl_1{\cdot}0.5CH_2Cl_2$: C, 66.51 (66.31); H, 4.17 (4.47); N, 4.70 (5.47).

Preparation of [Ru(STTP)(CO)(NO_3)] (2). In a Schlenk flask, [Ru(STTP)(CO)Cl] (**1**; 0.45 g, 0.529 mmol) and $AgNO_3$ (0.9 g, 5.29 mmol) dissolved in anhydrous dichloromethane (25 mL) under N_2 were allowed to stir at room temperature for 5 h. The resulting solution was filtered through a sinter-glass filter to remove unreacted $AgNO_3$ and AgCl. The filtrate was concentrated under reduced pressure on a rotovap, and *n*-hexane was added to precipitate the product. The resulting black solid of **2** was filtered and dried in vacuo. Yield: 0.3032 g (63%). ^{1}H NMR (200 MHz, 25 °C, chlororform-*d*, ppm): 9.32 (s, 2H, *β*-thiophene-H), 8.83 (d, *J* = 6.9 Hz, 2H, tolyl-H), 8.72 (m, 4H, *β*-pyrrole-H), 8.64 (s, 2H, *β*-pyrrole-H), 8.14 (dd, 2H, tolyl-H), 8.02 (d, *J* = 9.5 Hz, 2H, tolyl-H), 7.78 (d, *J* = 7.8 Hz, 2H, tolyl-H), 7.48 (m, 8H, tolyl-H), 2.69 (s, 12H, CH_3). UV−vis in CH_2Cl_2 [λ_{max}, nm, (log ε)]: 432 (4.93), 562 (3.86), 681 (3.69). Infrared (KBr, cm^{-1}): ν(CO) = 1965, ν(NO) = 1279, $\nu_s(NO_2)$ = 1385, $\nu_a(NO_2)$ = 1468. Elemental Anal. Calcd. (found) for $Ru_1C_{49}H_{36}N_4S_1O_4{\cdot}0.2CH_2Cl_2$: C, 66.03 (66.20); H, 4.10 (4.20); N, 6.26 (6.72).

Preparation of [Ru(STTP)(CO)(NO_2)] (3). In a Schlenk flask, [Ru(STTP)(CO)Cl] (**1**; 0.21 g, 0.246 mmol) and $AgNO_2$ (0.38 g, 2.47 mmol) dissolved in dichloromethane (25 mL) under N_2 were allowed to stir under ambient temperature for 9 h. Following the workup procedures as described for **2**, black solid **3** was obtained. Yield: 0.117 g (55%). ^{1}H NMR (200 MHz, 25 °C, chlororform-*d*, ppm): 9.33 (s, 2H, *β*-thiophene-H), 8.84 (d, *J* = 7.7 Hz, 2H, tolyl-H), 8.73 (dd, 4H, *β*-pyrrole-H), 8.66 (s, 2H, *β*-pyrrole-H), 8.16 (d, *J* = 6.8 Hz, 2H, tolyl-H), 8.06 (d, *J* = 7.2 Hz, 2H, tolyl-H), 7.79 (d, *J* = 7.3 Hz, 2H, tolyl-H), 7.51 (m, 8H, tolyl-H), 2.69 (s, 12H, CH_3). UV−vis in CH_2Cl_2 [λ_{max}, nm, (log ε)]: 432 (4.43), 581 (3.46), 682 (3.29). Infrared (KBr, cm^{-1}): ν(CO) = 1977, $\nu_a(NO_2)$ = 1366, $\nu_s(NO_2)$ = 1323. Elemental Anal. Calcd. (found) for $Ru_1C_{49}H_{36}N_4S_1O_3{\cdot}2CH_2Cl_2$: C, 59.36 (58.73); H, 3.91 (3.91); N, 5.43 (6.80).

Preparation of [Ru(STTP)(CO)(N_3)] (4). [Ru(STTP)(CO)Cl] (**1**; 0.2 g, 0.235 mmol) and NaN_3 (0.153 g, 2.35 mmol) dissolved in dry dichloromethane (25 mL) were allowed to stir at room temperature for 4 h. The resulting solution was filtered. The filtrate was concentrated under reduced pressure, and *n*-hexane (5 mL) was added. The solution was then stored in a freezer. A black precipitate formed overnight and was filtered and dried in vacuo to give black solid **4**. Yield: 0.144 g (72%). ^{1}H NMR (200 MHz, 25 °C, chloroform-*d*, ppm): 9.26 (s, 2H, *β*-thiophene-H), 8.64 (m, 4H, *β*-pyrrole-H), 8.58 (s, 2H, *β*-pyrrole-H), 8.07 (m, 6H, tolyl-H), 7.73 (d, *J* = 8.0 Hz, 2H, tolyl-H), 7.50 (m, 8H, tolyl-H), 2.67 (s, 12H, CH_3). UV−vis (CH_2Cl_2) [λ_{max}, nm, (log ε)]: 440 (4.81), 571 (3.82), 687 (3.63). Infrared (KBr, cm^{-1}): ν(CO) = 1958, ν_a(azido) = 2035, ν_s(azido) = 1262. Elemental Anal. Calcd. (found) for $Ru_1C_{49}H_{36}N_6S_1O_1{\cdot}0.5CH_2Cl_2{\cdot}0.5C_6H_{14}$: C, 66.83 (66.42); H, 4.70 (4.37); N, 8.91 (8.53).

Preparation of [Ru(STTP)Cl_2] (5). STTPH (0.33 g, 0.479 mmol) and [Ru(COD)Cl_2] (0.6 g, 2.87 mmol) dissolved in *o*-dichlorobenzene (200 mL) were allowed to stir under reflux for 5 h. The completion of the reaction was monitored by UV−vis spectroscopy. The resulting solution was filtered through Celite to remove excess [Ru(COD)Cl_2], and the solvent was removed under reduced pressure. The crude product was recrystallized from CH_2Cl_2/*n*-hexane to afford black solid **5**. Yield: 0.33 g (80%). UV−vis in CH_2Cl_2 [λ_{max}, nm, (log ε)]: 448 (4.74). Elemental Anal. Calcd. (found) for $Ru_1C_{49}H_{36}N_3S_1Cl_2{\cdot}1.2CH_2Cl_2{\cdot}0.5C_6H_{14}$: C, 62.90 (62.16); H, 4.50 (4.88); N, 4.14 (4.20).

Preparation of [Ru(S_2TTP)(NO_3)$_2$] (6). In a Schlenk-flask, [Ru(S_2TTP)Cl_2][25] (0.126 g, 0.144 mmol) and $AgNO_3$ (0.3 g, 1.77 mmol) were dissolved in 25 mL of anhydrous CH_2Cl_2 under nitrogen. After stirring for 4 h at ambient temperature, the residual $AgNO_3$ was filtered through a patch of Celite under a nitrogen atmosphere. The resulting solution was concentrated to about 5 mL, and *n*-hexane was

Table 1. Crystal Data and Structure Refinement for Ruthenium Complexes 1−7[a]

	1	2	3	4	5	6	7
formula	$C_{50}H_{38}Cl_3N_3ORuS$	$C_{50}H_{38}Cl_2N_4O_4RuS$	$C_{50}H_{38}Cl_2N_4O_3RuS$	$C_{49}H_{36}N_6ORuS$	$C_{48}H_{36}Cl_2N_3RuS$	$C_{48}H_{36}N_4O_6RuS_2$	$C_{74}H_{60}N_2RuS_2Se_4$
Mr	936.31	962.87	946.87	857.97	858.83	930.00	1458.27
cryst syst	monoclinic	monoclinic	monoclinic	triclinic	monoclinic	orthorhombic	monoclinic
group	$C2/m$	$C2/m$	$C2/m$	$P\bar{1}$	$C2/m$	$Pnnm$	$P2_1/n$
a, Å	21.5664(17)	22.6857(13)	21.877(4)	13.2450(10)	21.218(2)	18.6072(17)	9.171(2)
b, Å	17.0892(14)	17.1532(11)	17.060(3)	14.4126(10)	16.921(2)	7.8135(7)	26.666(7)
c, Å	15.4327(12)	15.5257(9)	15.357(3)	15.1075(11)	15.4948(16)	17.3417	13.984(4)
α, deg	90	90°	90	68.8070(10)	90	90	90
β, deg	117.0030(10)	119.1450(10)	116.90(3)	71.687(2)	116.673(3)	90	93.957(5)
γ, deg	90	90	90	76.3000(10)	90	90	90
V, Å^3	5067.7(7)	5276.6(5)	5111.3(18)	2527.8(3)	4970.9(9)	2521.3(4)	3411.6(15)
Z	4	4	4	2	4	2	2
ρ_{calcd}	1.227	1.234	1.230	1.127	1.148	1.225	1.420
T, K	298	295	298	298	298	298	293
total reflns	6043	6164	6010	11233	5080	2996	7788
obsd reflns	4176	4537	4521	7319	1621	1962	3938
R_1	0.0489	0.0536	0.0384	0.0448	0.0550	0.0543	0.0611
wR_2	0.1427	0.1885	0.1106	0.1195	0.1574	0.1450	0.1881

[a] $R_1 = \sum||F_o| - |F_c||/\sum|F_o|$; $wR_2 = [\sum w(F_o^2 - F_c^2)^2/\sum w(F_o^2)^2]^{1/2}$; $w = 1/\sigma^2(|F_o|)$.

dx.doi.org/10.1021/ic200977n|Inorg. Chem. 2011, 50, 11947–11957

Scheme 1

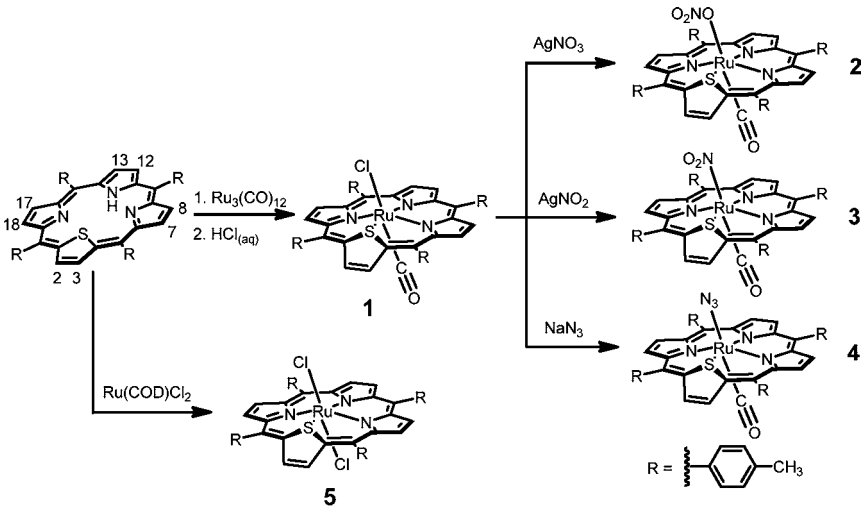

added dropwise. The crystalline precipitate was collected and dried in vacuo to afford black solid **6**. Yield: 0.105 g (78%). ^{1}H NMR (300 MHz, 25 °C, chloroform-*d*, ppm): 8.90 (s, 1H, *β*-thiophene-H), 8.85 (s, 1H, *β*-thiophene-H), 8.79 (s, 2H, *β*-pyrrole-H), 8.20−8.40 (br, 4H, tolyl-H), 7.96 (ABq, 2H, $\Delta\delta_{AB}$ = 0.04, J_{AB} = 6 Hz), 7.87 (s, 2H, *β*-pyrrole-H), 7.10−7.70 (br, 12H, tolyl-H), 2.56 (s, 12H, CH_3). UV−vis in CH_2Cl_2 [λ_{max}, nm, (log ε)]: 467 (4.67), 556 (4.05), 593 (3.95), 822 (3.67). Infrared (KBr, cm^{-1}): $\nu_a(NO_2)$ = 1467, $\nu_s(NO_2)$ = 1384, ν(NO) = 1262. Elemental anal. calcd. (found) for $RuC_{48}H_{36}N_4S_2O_6$·2.4 CH_2Cl_2: C, 53.39 (53.34); H, 3.63 (3.64); N, 4.94 (5.26).

Preparation of [Ru(S$_2$TTP)(PhSeCH$_2$SePh)$_2$] (7). In a $N_{2(g)}$-filled Schlenk flask, [Ru(S$_2$TTP)Cl$_2$] (0.1 g, 0.114 mmol) and NaSePh (0.3 g, 1.68 mmol) were dissolved in 25 mL of anhydrous CH_2Cl_2. The solution was allowed to stir for 8 h at ambient temperature, and the color of the solution changed from deep yellow-green to dark-red. The resulting solution was filtered through Celite under N_2, and the solvent was removed under reduced pressure. An analytically pure compound was obtained from recrystallization of the crude compound from CH_2Cl_2/hexane/DMF. Yield: 0.129 g (78%). UV−vis in CH_2Cl_2 [λ_{max}, nm, (log ε)]: 343 (sh, 4.24), 401 (4.44). Elemental Anal. Calcd. (found) for $RuC_{74}H_{60}N_2S_2Se_4$·1.5 CH_2Cl_2·C_3H_7NO: C, 58.37 (58.60); H, 4.05 (4.03); N, 1.82 (1.88).

X-Ray Crystallography. Diffraction measurements for complexes **1**−**7** were carried out on a Bruker SMART 1000 or an Apex CCD diffractometer equipped with graphite-monochromated Mo Kα radiation (λ = 0.71073 Å). Crystallographic data and data collection parameters are summarized in Table 1. Structural refinements were performed by means of SHELXTL software.[26] Phase determination for the structures was done through the Patterson method and expanded using Fourier techniques. Least-squares refinement of the positional and anisotropic thermal parameters for the contribution of all non-hydrogen atoms and fixed hydrogen atoms was based on F^2. A SADABS[27] absorption correction was made. The weighted R factor (wR_2) and goodness of fit (GOF) were against F^2. The threshold expression of $F^2 > 2\sigma(F^2)$ was used only for calculating R factors and is not relevant to the choice of reflections for refinement.

Theoretical Calculation. Theoretical calculations were performed with the Gaussian 03 revision D.02 program.[28] Starting geometries were obtained from the crystal structures **1**−**4**. Geometry optimizations were performed at the restricted Hartree−Fock level under an unconstrained C1 symmetry. Preliminarily optimized structures for complexes **1**−**4**, after the Hartree−Fock calculation, were fully optimized using the DFT method at the B3LYP[29−32] level with 6-31+G** as a basis set for light atoms (C, H, N, and O), MIDIX for chloride, and LanL2DZ[33,34] for ruthenium atom. Harmonic vibrational frequencies were calculated using analytical second derivatives for all systems. Vibrational frequencies were calculated for all optimized structures to confirm that the obtained geometries represent true minima without an imaginary frequency. In all calculations, convergence was reached when the relative change in the density matrix between subsequent iterations was less than 1×10^{-8}. A time-dependent density functional theory (TDDFT) approach was used for the prediction of UV−vis spectra of ruthenium thiaporphyrin complexes. Molecular geometries were optimized using the above-mentioned exchange-correlation functional and basis sets, coupled with a self-consistent reaction field method (SCRF), specifically, Tomasi's PCM,[35] in dichloromethane (ε = 8.93). Molecular orbitals were visualized using *Gauss View*, revision 3.0.9.

RESULTS AND DISCUSSION

Ruthenium Carbonyl Thiaporphyrin Complexes. Either [Ru$_3$(CO)$_{12}$] or [Ru(COD)Cl$_2$] was used as a starting metal source for the metalation of thiaporphyrin through oxidative insertion. The use of [Ru$_3$(CO)$_{12}$] as the ruthenium source introduced a carbonyl to the axial position, while a high-valent Ru(III)−thiaporphyrin was obtained when [Ru(COD)Cl$_2$] was used as the starting compound. As shown in Scheme 1, the refluxing of STTPH and [Ru$_3$(CO)$_{12}$] in *o*-dichlorobenzene followed by an extraction using aqueous HCl solution affords [Ru(STTP)(CO)Cl] (**1**). A temperature above 150 °C appeared to be a prerequisite for ruthenium metalation. No product was observed when solvents with a lower boiling point, such as toluene, benzene, or $CHCl_3$, were used. Alternatively, ruthenium metalation can be achieved with comparable yields using mesitylene as the solvent, albeit a longer reaction time is required. Compound **1**, which is stable under the solution state in the ambient atmosphere, had a good solubility in dichloromethane and chloroform but moderate solubility in tetrahydrofuran or methanol. Dechlorination of **1** with $AgBF_4$ followed by treatment with an oxidant, e.g., H_2O_2 or *m*-chloroperbenzoic acid (*m*-CPBA), under room temperature for 24 h resulted in a product lacking a carbonyl group stretching frequency. However, no reaction between **1** and the oxidant can be observed without prior dechlorination by the silver ion, implying that axial chloride increases the stability of **1**.

In comparison with the *Soret* band at 429 nm and *Q*-bands at 414, 550, 618, and 678 nm for the free base STPPH, the absorption spectrum for **1** with a λ_{max} at 433 nm for the *Soret* band and 575 and 690 nm for *Q* bands is significantly red-shifted. The red-shift might be attributed to the nonplanarity of

dx.doi.org/10.1021/ic200977n | *Inorg. Chem.* 2011, 50, 11947−11957

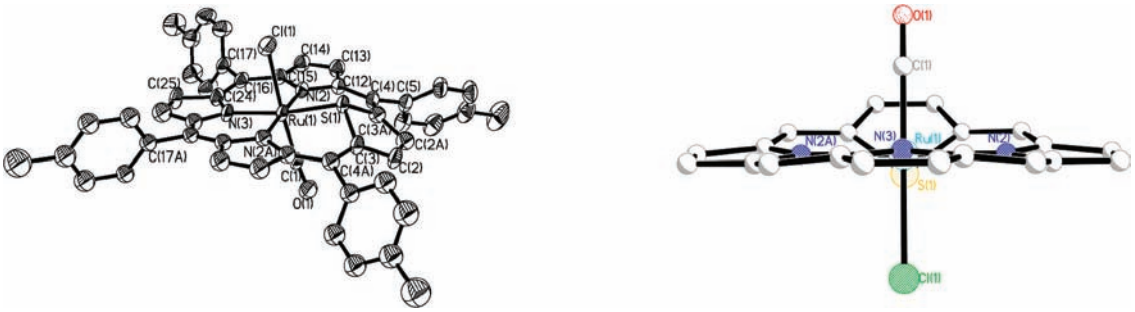

Figure 1. Molecular structure of [Ru(STTP)(CO)Cl] (**1**) in 30% ellipsoids (left) and the side view of **1** with phenyl rings omitted for clarity (right).

the thiaporphyrin core after ruthenium metalation, suggesting the presence of the hybrid orbital deformation (HOD) effect.[36] The NMR pattern of complex **1** is consistent with a C_s symmetrical molecule with axial ligands, the ruthenium center, the sulfur atom, and a pyrrolic nitrogen embedded in a plane of symmetry. *AB* quartet resonances at 8.66 and 8.61 ppm arising from H_7, H_8, H_{17}, and H_{18} (see Scheme 1) on β-pyrrolic carbons neighboring the thiophene rings were observed. The protons on symmetry embedding thiophene and pyrrole rings were located at 9.26 and 8.57 ppm, respectively.

Single-crystal X-ray structure determination provides explicit information for the conformation of **1**. As shown in Figure 1, complex **1** displays a nonplanar thiaporphyrin macrocycle with the thiophene moiety tilted away from the mean porphyrinic plane. Values of deviations for thiophenic atoms from the mean plane defined by the tripyrrin moiety are as follows: S(1), −0.50 Å; C(3), 0.38 Å; C(2):, 1.03 Å. The ruthenium atom sits nearly coplanar with the mean plane with a deviation of 0.0030 Å. The angle of 59.02° between the C(3)−S(1)−C(3A) plane and the equatorial plane consisting of Ru(1) and coordinating atoms falls in the middle of 45.9° for [Ni^{I}(SDPDTP)Cl][19] and 69.5° for [Fe^{II}(STPP)Cl].[18] Similar to other metal−thiaporphyrin complexes, the five-member ring of thiophene in **1** is puckered with an angle of 16.05° between C(3)−S(1)−C(3A) and C(3)−C(2)−C(2A)−C(3A)-containing planes. The ruthenium(II) complex **1** possesses one chloro and one carbonyl as the axial ligands. The ν(CO) was located at 1956 cm^{-1}. The carbonyl group sits at the opposite side of the thiophenic sulfur atom with an angle of 173.7(4)° for Ru(1)−C(1)−O(1). A vector defined by atoms of axial ligands Cl(1), Ru(1), and C(1) exhibits a tilting angle of 8.07° away from the normal of the plane defined by the tripyrrin moiety. The distances of 2.044(3) and 2.077(2) Å for Ru−N are close to an average of 2.049 Å for Ru^{II}−N bonds among reported ruthenium porphyrin complexes. Furthermore, distances of 1.834(4) and 1.114(5) Å for the bond lengths of Ru(1)−C(1) and C(1)−O(1), respectively, fall in the range of distances (1.762−1.959 Å for Ru−C and 0.961−1.188 Å for C−O) reported for available ruthenium−carbonyl porphyrin complexes. The Ru−Cl distance of 2.469(1) Å in **1** is significantly longer than the average of 2.398 Å for structurally available nonporphyrinic Ru^{II} complexes containing one chloride, one carbonyl, and at least three nitrogens in the coordination sphere deposited in the Cambridge Structural Database (CSD).[37] Although there is no precedent for ruthenium porphyrins with a Cl^- and a CO at the *trans* positions, both the unexpectedly long Ru−Cl bond and the normal Ru−C and C−O bond lengths for the Cl−Ru−(CO) moiety of **1** suggest a weakened interaction between Ru and Cl.

Substitution of Axial Chloride on [Ru(STTP)(CO)Cl] with NO_3^-, NO_2^-, or N_3^- through Metathesis Reactions. The axial chloride in **1** allows the preparation of a series of ruthenium thiaporphyrin complexes through a metathesis reaction, as shown in Scheme 1. Ruthenium(II) thiaporphyrin complexes [Ru(STTP)(CO)X] (X = NO_3^- (**2**), NO_2^- (**3**), and N_3^- (**4**)) were obtained in moderate yield from the reaction of **1** with corresponding silver(I) salts (for **2** and **3**) or sodium salt (for **4**) in CH_2Cl_2. The azido product **4** was stable in both solid and solution states under aerobic conditions. Black crystals of **4** were readily obtained through crystallization from a near-saturated CH_2Cl_2 solution of **4**. The nitrato (**2**) and nitro (**3**) complexes, however, are less stable; demetalation proceeded slowly in the solution of **2** and **3** under atmospheric conditions.

Complexes **2**, **3**, and **4** were characterized by means of UV−vis, NMR, and IR spectroscopies and single-crystal X-ray structural determination. As shown in Figure 2, the

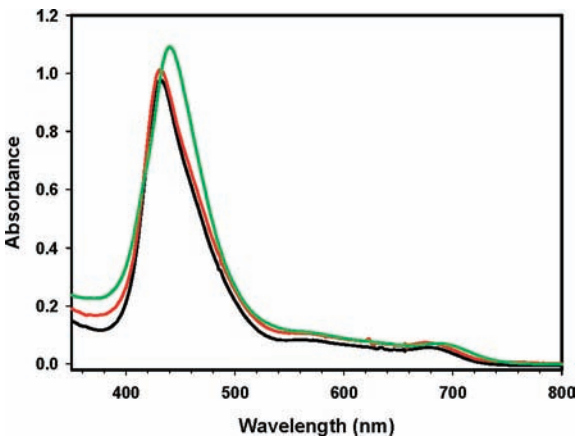

Figure 2. The absorption spectra of **2** (black line), **3** (red line), and **4** (green line).

pseudohalide−ruthenium−carbonyl− thiaporphyrins exhibit similar UV−vis absorption patterns with an asymmetric *Soret* band located at 432 nm for **2** and **3** and 440 nm for **4**. The *Q*-bands at around 570 and 680 nm for **2**−**4** are weak and broadened. Metal-to-ligand charge transfer (MLCT) bands for porphyrin complexes are generally difficult to identify because of overlapping with intense porphyrinic $\pi\rightarrow\pi^*$ transitions. The asymmetric character of *Soret* bands with an observable tailing at around 500 nm for **2**−**4** might imply the overlap of the MLCT absorption with the *Soret* band. Analyzing the potential electronic transitions obtained from the theoretical calculations revealed a charge-transfer band around 480 nm for all ruthenium−carbonyl−thiaporphyrin complexes, which sup-

dx.doi.org/10.1021/ic200977n | *Inorg. Chem.* 2011, 50, 11947−11957

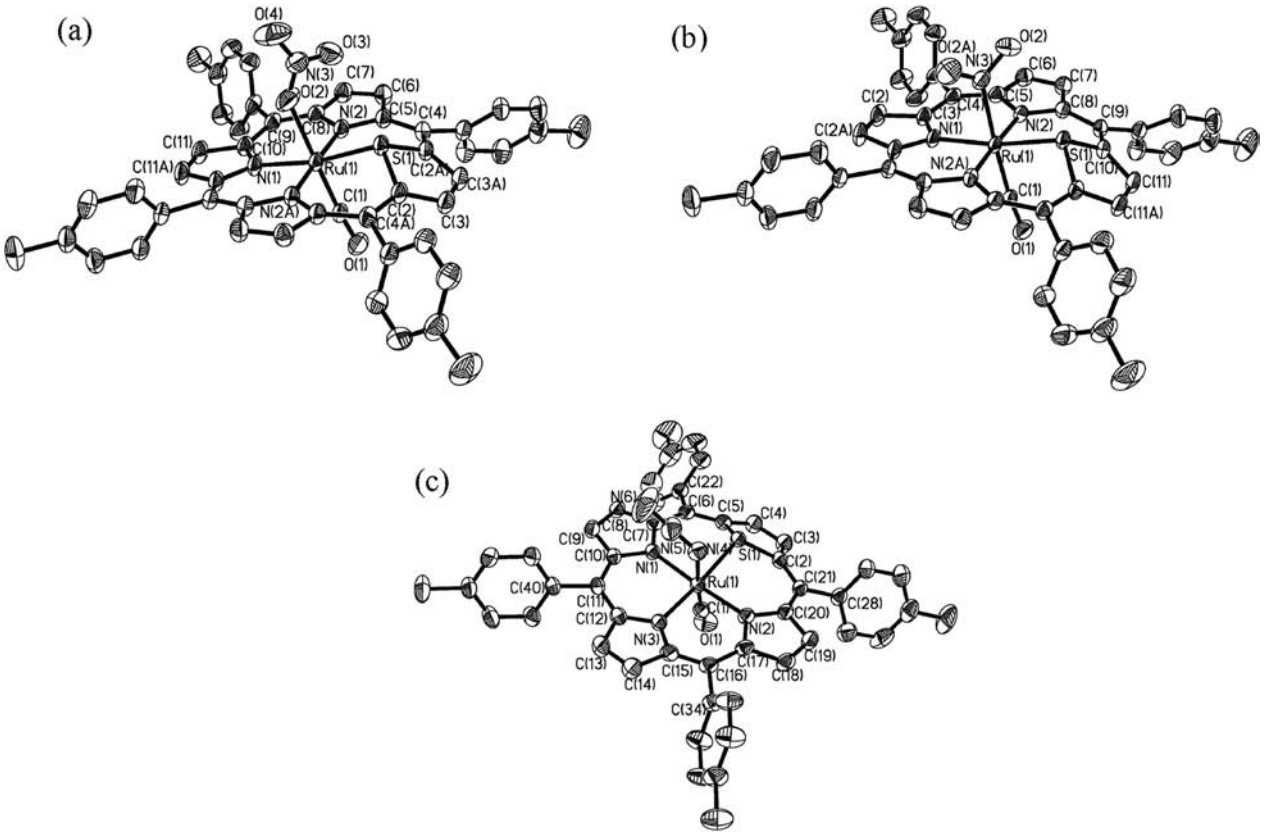

Figure 3. The molecular structures of **2** (a), **3** (b), and **4** (c) in 25% ellipsoids. Only one of the two disordered positions for **2** and **3** was presented. Hydrogen atoms are omitted for clarity.

ports the speculation that porphyrinic $\pi\rightarrow\pi^*$ transitions overlap with a change-transfer band, resulting in tailing *Soret* bands. On the other hand, the UV−vis absorptions of **1**−**4** are insensitive to the axial pseudohalides. A similar phenomenon has been observed in a series of ruthenium−nitrosyl porphyrin complexes [Ru(porphyrin)(NO)(X)] (X = NO_3^-, H_2O, NCS^-, Cl^-, NO_2^-, NSO^-, N_3^-, OH^-, OMe^-, SH^-),[27] and the insensitivity has been attributed to the dominance of the strong π-accepting ligand on the interaction between axial ligands and the ruthenium center.[38]

In the ^{1}H NMR spectra of **2**−**4**, singlet resonances at 9.32 and 8.64 ppm for **2** and at 9.33 and 8.66 ppm for **3** resulted from β-thiophenic and β-pyrrolic protons, respectively, are all downfield shifted compared with the corresponding resonances of 9.26 and 8.57 ppm for **1**. The largest downfield shifted meso-tolyl proton resonance was at 8.06 ppm for **1** and 8.07 ppm for **4**, whereas for **2** and **3** unusually downfield shifted doublet resonances for *meso* tolyl groups at 8.83 ppm and 8.84 ppm, respectively, were observed. The extra downfield shifting of *ca.* 0.75 ppm in **2** and **3** for the *meso*-tolyl resonance indicates either an intramolecular or an intermolecular weak hydrogen-bonding interaction from the nitrato or nitro group to aromatic protons on tolyl groups.

Characteristic vibrational modes from axial ligands in the infrared spectra of **2**−**4** provide fingerprint-like peaks for understanding the bonding modes of axial ligands. Specifically, the difference of $\nu_a(NO_2)$ and $\nu_s(NO_2)$ ($\Delta(\nu_a - \nu_s)$) has been used to differentiate chelating modes of NO_3^- and NO_2^- in their metal complexes. The infrared spectrum of nitrato complex **2** showed characteristic bands of 1468, 1385, and 1279 cm^{-1}, which were assigned to $\nu_a(NO_2)$, $\nu_s(NO_2)$, and ν(NO), respectively. According to those reported cases, the unidentate chelating of nitrato in $[Ni(en)_2(NO_3)_2]$ gave a $\Delta(\nu_a - \nu_s)$ = 115 cm^{-1}, while a much larger value of 186 cm^{-1} was obtained from the nitrato group with a bidentate chelating mode in $[Ni(en)_2(NO_3)]ClO_4$.[39] Consequently, the small $\Delta(\nu_a - \nu_s)$ value of 83 cm^{-1} in the nitrato complex **2** indicates a unidentate coordination mode. The $\nu_a(NO_2)$ and $\nu_s(NO_2)$ for the nitro group in complex **3** were located at 1366 and 1323 cm^{-1}, respectively. These values are in the lower energy regions of 1470−1370 cm^{-1} for $\nu_a(NO_2)$ and 1340−1320 cm^{-1} for $\nu_s(NO_2)$ and are consistent with stretching frequencies of a N-bound NO_2^-.[40] The characteristic IR frequencies of azido complex **4** were located at 2035 cm^{-1} for $\nu_a(N_3)$ and 1262 cm^{-1} for $\nu_s(N_3)$. These frequencies fall in the normal region for these linear triatomic pseudohalogeno groups but are lower than 2048 and 1291 cm^{-1} for $\nu_a(N_3)$ and $\nu_s(N_3)$, respectively, in the complex $[Ru(TTP)(NO)(N_3)]$.[38]

Since ν(CO) is highly sensitive to the electronic structure of the carbonyl complex, the ν(CO) values can be used to gauge the electron-donating ability of the ligand *trans* to the carbonyl group. As the electron-donating ability of the *trans* ligand increases, the increased π back-bonding from ruthenium to carbonyl group results in a lower ν(CO). The comparison of the ν(CO) values among [Ru(STTP)(CO)X] demonstrates a proportional correlation of the ν(CO) with the electron-donating ability of *trans* ligands. Complex **1** with a chloride *trans* to CO exhibited the lowest ν(CO) at 1956 cm^{-1}. These values increased to 1958 cm^{-1} for the azido complex, 1965 cm^{-1} for the nitrato complex, and 1977 cm^{-1} for the nitro complex, indicating electron-donating ability in a spectrochemical series of $Cl^- \sim N_3^- > NO_3^- > NO_2^-$ for the ruthenium−

dx.doi.org/10.1021/ic200977n | *Inorg. Chem.* 2011, 50, 11947−11957

Table 2. Selected Bond Distances and Angles for 1–4

	1	2	3	4	5
			bond distances		
Ru–N(Por)	2.044(3)	2.050(4)	2.047(2)	2.037(2)	2.013(7)
	2.077(2)	2.086(3)	2.071(2)	2.068(2)	2.057(5)
				2.070(2)	
Ru–S	2.2453(10)	2.2436(11)	2.2436(9)	2.2240(7)	2.251(2)
C–O	1.114(5)	1.148(6)	1.137(4)	1.149(4)	
Ru–C(CO)	1.834(4)	1.822(5)	1.862(3)	1.834(3)	
Ru–X_{axial}	2.4694(14)	2.120(5)	2.145(3)	2.155(3)	2.320(2)
					2.356(2)
			bond angles		
N(Por)–Ru–N(Por)	91.26(5)	91.28(6)	91.43(4)	91.43(9)	91.44(13)
	177.48(10)	177.23(11)	177.14(9)	91.53(9)	176.0(3)
				176.73(8)	
S–Ru–N(Por)	88.76(5)	88.65(6)	88.58(4)	88.65(6)	88.71(13)
	171.47(10)	169.86(12)	170.24(8)	88.19(6)	174.22(19)
				169.61(7)	
C–Ru–X_{axial}	175.78(12)	178.83(18)	176.32(12)	176.06(11)	177.36(9)[d]
Ru–C–O	173.7(4)	174.9(4)	172.7(3)	173.1(3)	
Φ^a (deg)	16.05(15)	16.99(21)	15.98(11)	15.67(13)	16.36(29)
$\Delta(Ru)^b$ (Å)	0.0030	0.038	0.0074	0.0136	0.0649
$\Delta(S)^b$ (Å)	0.50	0.50	0.52	0.54	0.50
Λ^c (deg)	59.02(8)	59.81(9)	58.39(7)	56.85(8)	59.52(21)

[a]Dihedral angle between planes of C_α–C_β–C_β–C_α and C_α–S–C_α. [b]Atomic deviation from mean plane defined by the tripyrrin moiety. [c]Angle between plane of C_α–S–C_α and plane of S–Ru–N(Por).

carbonyl–thiaporphyrins. It is noteworthy that the N-bound nitro group has been considered an extremely good π-acceptor in the five coordinated complex $[Fe(TpivPP)(NO_2)]^-$ according to the short bond distance of 1.849 Å for Fe–$N(NO_2)$.[41] However, the strong π-accepting nature of the nitro group has been found to substantially diminish in six-coordinate nitro complexes.[42] In conjunction with the longer Ru–$N(NO_2)$ distance and nearly constant bond lengths of Ru–X (X = O for nitrato and N for nitro and azido) as described below, we conclude that it is the electron-donating character but not the π-accepting ability of the ligand *trans* to CO which dominates the values of ν(CO).

To corroborate the molecular conformation, the single-crystal structures of **2**, **3**, and **4** were obtained and displayed in Figure 3. Selected bond distances and angles as well as important structure parameters for complexes **1**–**4** are listed in Table 2. Compounds **2** and **3** crystallized in the monoclinic $C2/m$ space group, while **4** crystallized in triclinic $P\bar{1}$. In the structure of **2**, atoms of Ru, CO, and two of the oxygens from nitrato group sit on the special positions to generate, from symmetry operation, not only the other half molecule but also a disordered NO_3^- with 50% occupancy. The nitro group in complex **3** is also disordered in two positions with 50% occupancy on each site. Overall, in addition to the different pseudohalide coordination, the conformation of the ruthenium–carbonyl–thiaporphyrin moiety for **2**, **3**, and **4** resembles that of **1**. As predicted from IR spectra, the nitrato ligand in **2** adopted an O-bound monodentate binding mode, while an N-bound nitro group was observed in the structure of **3**. To the best of our knowledge, complex **3** is the first structurally characterized N-bound ruthenium nitro porphyrin complex, and there is no precedent for a crystal structure for a ruthenium porphyrin complex containing either a nitrato or an azido as the axial ligand.

As listed in Table 2, Ru–N(Por) bond distances for complexes **2**, **3**, and **4** are in the range of 2.037(2)–2.086(3) Å, which are in the normal range for ruthenium porphyrin complexes. The bond distance of Ru–N(Por) *trans* to the Ru–S is significantly shorter than the other two Ru–N(Por) bonds, presumably due to the weakened Ru–S bond under the pyramidal coordination geometry. In all ruthenium–thiaporphyrin complexes, ruthenium centers are nearly coplanar with the mean plane of the tripyrrin. Thiophenic sulfur atoms deviate from the mean-plane of the tripyrrin toward nitrato, nitro, and azido with values of 0.50, 0.50, and 0.52 Å for **2**, **3**, and **4**, respectively. The Ru–$O_{nitrato}$ bond distance of 2.120(5) Å in complex **2** is longer than the reported distance of 2.059 Å for Ru–$O_{nitrato}$ in *cis*-$[Ru(NO)(NO_3)(bpy)_2](ClO_4)_2$.[43] Also, the Ru–$N_{nitro}$ distance of 2.145(3) Å in **3** is longer than those of 2.066 and 2.071 Å for Ru–N_{nitro} in $[Ru(PC)(NO_2)_2]$ (PC = phthalocyaninato).[44] These relatively long Ru–$O_{nitrato}$ and Ru–N_{nitro} bonds indicate that the electron density on Ru–O and Ru–N bonds is outcompeted by the back-bonding from the ruthenium ion to the carbonyl antibonding orbital. Complex **2**, which has a nitrato axial ligand, gives the shortest Ru–C(CO) distance, and longer C–O distances are seen in **1**–**4**, implying the utmost back-bonding interaction among the complexes studied herein.

A ubiquitous phenomenon in the crystal structures of ruthenium–carbonyl–thiaporphyrins is that the deviating thiophenic sulfur is always leaning toward chloride/pseudohalides. Results of theoretical calculations rationalize this tendency. As listed in Table 3, the total-energy difference between two scenarios, thiophenic sulfur directed toward axial chloride/pseudohalides (observed) and the sulfur directed toward the axial carbonyl group (proposed), clearly indicates that the former one is always preferable over the latter one, which is consistent with the observation in solid state structures. For example, in the case with the largest energy

dx.doi.org/10.1021/ic200977n | *Inorg. Chem.* 2011, 50, 11947–11957

Table 3. Total Electronic Energies (E_{total}), Zero Point Vibrational Energies (E_{total} + ZPV), and Their Relative Differences in Energies between Two Potential Thiophene Orientations (E_{rel})

compounds[a]	E_{total} in Hartree	E_{total} + ZPV	E_{rel} in kcal/mol
1	−1997.13186895	−1996.850819	0.0
1a	−1997.13054609	−1996.849367	0.91
2	−1819.35610923	−1819.060129	0.0
2a	−1819.35014942	−1819.054025	3.83
4	−1703.24395868	−1702.951729	0.0
4a	−1703.24386005	−1702.951508	0.13

[a]A bend nitrito ligand with an angle of 54° between nitrito O−N−O plane and the porphyrinic tripyrrin plane was obtained from the structural optimization of **3**. This optimized structure apparently is one of the stabilization forms but is significantly different from the crystal structure. Therefore, data obtained for **3** were not included here.

difference (**2** and **2a**), the observed conformer with the sulfur directed toward the nitrato group is 3.83 kcal/mol lower in energy than the proposed one. Even in the azido case with only a minute energy difference (**4** and **4a**), the observed conformer is 0.13 kcal/mol more stable than the proposed one. Further analysis on the optimized structures reveals that the stable conformers exhibit shorter Ru−CO bond distances but longer C−O and Ru−S bond distances in comparison with the higher energy ones, suggesting that the observed conformers show a stronger ruthenium-to-carbonyl back-bonding interaction than proposed ones.

Synthesis of Higher Valence [Ru^{III}(STTP)Cl$_2$] (5). Ru^{III}−thiaporphyrin complex [Ru(STTP)Cl$_2$] (**5**) was synthesized by treating STTPH with Ru(COD)Cl$_2$ in *o*-dichlorobenzene in moderate yield. The absorption spectrum with the *Soret* band at 446 nm is slightly red-shifted relative to the Ru^{II} thiaporphyrin complexes **1**−**4**. In contrast to the broad and asymmetric *Soret* bands in **1**−**4**, the *Soret* band in **5** is sharp and symmetrical, and no obvious Q-band can be observed in the lower energy region. ^{1}H NMR resonances of complex **5** were too broad to be observed because of the intrinsic paramagnetic characteristic. Complex **5** is stable under aerobic conditions in both solid and solution states, and no demetalation proceeded under examined conditions. The high stability of **5** allows the examination of redox processes by cyclic voltammetry. As shown in Figure 4, two reversible and one irreversible process were observed in the cyclic voltammogram of **5**. The half-wave potential at +1.083 V, which is close to +1.03 V for the first oxidation potential of the free-base thiaporphyrin, presumably resulted from a thiaporphyrin-centered oxidation. The other reversible process at $E_{1/2}$ = −0.123 V, which is considerably different from −1.065 V for a thiaporphyrin-centered reduction in STTPH, was assigned to the Ru^{3+}/Ru^{2+} redox couple. The irreversible process at −1.476 V, which is more negative than −1.065 V for the STTPH reduction, indicates that a more electron-rich species might be generated after the Ru^{III} → Ru^{II} reduction process. Since there is no observable redox potential corresponding to a Ru^{II} → Ru^{I} process, it is likely that the [Ru^{II}(STTP)Cl$_2$]$^-$ is not stable and readily demetalated to STTP$^-$. A similar reduction-promoting demetalation was observed in an earlier electrochemical study on [Cu(STTP)X] (X = Cl$^-$ or HCO$_3^-$).[45] A reduction potential with an $E_{1/2}$ value of −1.40 V, which is close to the −1.476 V observed in **5**, has been assigned as the addition of a second electron to the free

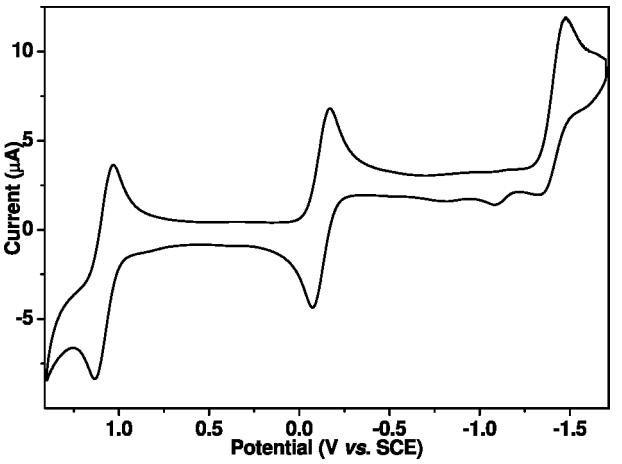

Figure 4. The cyclic voltammogram of **5** in THF with 0.1 M tetra-*n*-butylammonium hexafluorophosphate under a scan rate of 50 mV/s.

ligand after electrochemical demetalation of [Cu(STTP)X], a ·STTPH$^-$/STTPH^{2-} redox process.

Single-crystal X-ray structural determination, as shown in Figure 5, revealed that the neutral complex consists of two Cl$^-$

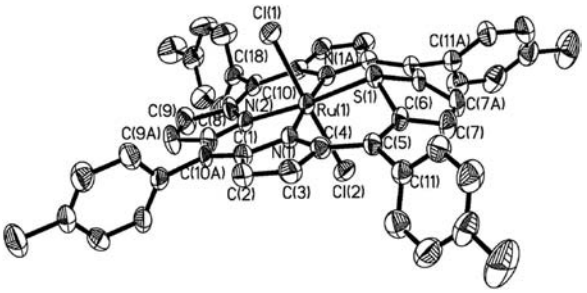

Figure 5. The molecular structure of **5** under 25% ellipsoids. Hydrogen atoms are omitted for clarity.

ligands coordinating at axial positions and one thiaporphyrin chelating in a tetradentate mode to give a formally Ru(III) complex. The bond lengths of Ru−Cl in **5** are 2.320(2) and 2.356 (2) Å, which are shorter than the 2.469(1) Å in **1**, as expected for a complex with the Ru^{III} oxidation state. As shown in Table 2, the distances of 2.013(7) and 2.057(5) Å for Ru−N(Por) are also slightly shorter than corresponding distances for Ru^{II}−N(Por). The Ru−S distance and bending angle of the thiophene ring in **5** are almost identical to those of Ru^{II} thiaporphyrin complexes, implying that a steric constraint instead of electrostatic interaction dominates the conformation of the thiophene moiety.

Preparation of Ruthenium Dithiaporphyrin Complexes with Nitrate or Bis(phenylseleno)methane As Axial Ligands. The free-base 5,10,15,20-tetra-*p*-tolyl-21,23-dithiaporphyrin, S$_2$TTP, was prepared via condensation of 2,5-bis(tolylhydroxylmethyl)thiophene and pyrrole using BF$_3$·OEt$_2$ as an acid catalyst followed by oxidation with DDQ. As sketched in Scheme 2, the reaction of [Ru(S$_2$TTP)Cl$_2$][25] with a large excess of AgNO$_3$ or NaSePh isolates [Ru(S$_2$TTP)-(NO$_3$)$_2$] (**6**) or [Ru(S$_2$TTP)(PhSeCH$_2$SePh)$_2$] (**7**), respectively, in 78% yields. Both complexes **6** and **7** were air-sensitive, and all preparations have been carried out under N$_2$. Complex **6** was stable in CH$_2$Cl$_2$ with no significant decomposition during the workup; however, passing the toluene or THF

dx.doi.org/10.1021/ic200977n | *Inorg. Chem.* 2011, 50, 11947−11957

Scheme 2

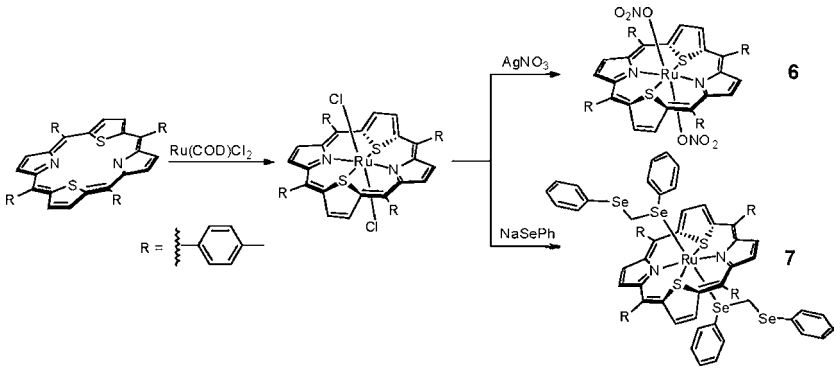

solution of **6** through Celite in an inert atmospheric drybox instantly produced **6** and free-base S_2TTP with a ratio of 1:1. The isolation of **7** from the reaction of [Ru(S_2TTP)Cl_2] and NaSePh was unexpected. Presumably, a concerted bond-breaking/formation between the intermediate, [Ru(S_2TTP)-(SePh)$_2$], and CH_2Cl_2 through a radical pathway results in the formation of $PhSeCH_2Cl$ and simultaneously reduces the ruthenium(II) complex to ruthenium(0). As $PhSeCH_2Cl$ possesses higher reactivity toward nucleophilic-attack substitution, the reaction of excess $PhSe^-$ and $PhSeCH_2Cl$ readily resulted in the formation of *bis*(phenylseleno)methane. Control studies to derive a plausible mechanism are described in detail in the following paragraphs.

Complex **6** exhibits absorption maxima at 467, 556, 593, and 816 nm (Figure 6) similar to the pattern of [Ru(S_2TTP)Cl_2],

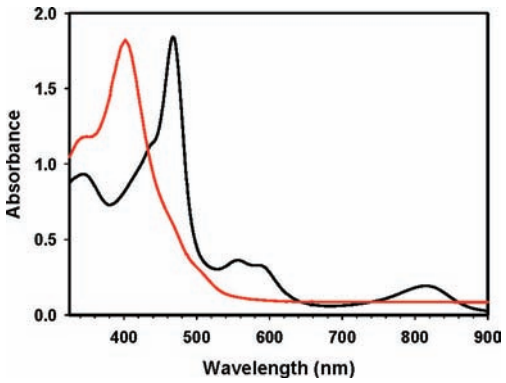

Figure 6. The absorption spectra of ruthenium dithiaporphyrin complex **6** (black) and **7** (red).

whereas the formally ruthenium(0) complex **7** gives a broad and unusually blue-shifted *Soret* band at 400 nm with no obvious *Q*-band. Complex **6** displayed IR absorption peaks at 1467 cm^{-1} for $\nu_a(NO_2)$, 1384 cm^{-1} for $\nu_s(NO_2)$, and 1262 cm^{-1} for ν(NO) with $\Delta(\nu_a - \nu_s)$ of 83 cm^{-1}, which are consistent with the values for a monodentate nitrato ligand. The NMR spectrum of **6** in $CDCl_3$ shows sharp peaks for β-thiophenic and β-pyrrolic protons, and resonances of *meso*-tolyl protons were broadened into three humps at 8.30, 7.57, and 7.32 ppm, showing that a twisting thiaporphyrin core results in a facile dynamic rotation of *meso*-tolyl rings at room temperature. The ^{1}H NMR signals of **7** were extremely broad between 6.50 and 8.75 ppm for β-thiophenic, β-pyrrolic, and *meso*-tolyl protons, and no further efforts were made to assign the resonances.

To provide more insight into the formation and coordination of *bis*(phenylseleno)methane, control reactions with or without the presence of [Ru(S_2TTP)Cl_2] were stoichiometrically and spectroscopically monitored. At room temperature, the reaction of NaSePh and CH_2Cl_2, without any metal complex or base, under anaerobic conditions for 12 h, isolated diphenyl diselenide and *bis*(phenylseleno)methane in low yields (12%). Noticeably, no reaction was observed when 2.0 equiv of NaSePh were reacted with [Ru(S_2TTP)Cl_2]. On the other hand, the reaction of 4.0 equiv of NaSePh with [Ru(S_2TTP)-Cl_2] in CH_2Cl_2 yielded an electronic absorption pattern with *Soret* band at 448 nm and *Q*-bands at 589 and 814 nm, which resembles those of [Ru(S_2TTP)Cl_2] and **6**, suggesting that the reaction might achieve [Ru^{II}(S_2TTP)(SePh)$_2$] through a metathesis reaction. Treatment of the reaction mixture with another 4.0 equiv of NaSePh, the UV−vis spectrum gradually shifted to that of complex **7**. The crude mixture from a reaction of [Ru(S_2TTP)Cl_2] and 14.7 equiv of NaSePh was extracted with hexane, and the GC-mass analysis identified $PhSeCH_2Cl$ (relative intensity: 100%), PhSeSePh (20%), and $PhSeCH_2SePh$ (77%) as three major products. Implications from the above-mentioned control reactions and the presence of a large amount of $PhSeCH_2Cl$ in the reaction mixture, which is not observed from the reaction of NaSePh and CH_2Cl_2 in the absence of [Ru(S_2TTP)Cl_2], are as follows: (1) reaction of [Ru^{II}(S_2TTP)(SePh)$_2$] and CH_2Cl_2 might result in a concerted formation of PhSe−CH_2Cl through homolytic cleavage of both axial Ru^{II}−SePh bonds with a concurrent reduction of Ru(II) to Ru(0); (2) reaction of the more reactive $PhSeCH_2Cl$ and $PhSe^-$ readily proceeded to form $PhSeCH_2SePh$ via a nucleophilic-attack pathway; (3) the Ru^0 intermediate, resulted from the reductive elimination of $PhSeCH_2Cl$, was stabilized by the coordination of *bis*(phenylseleno)methane, of which the vacant 3d orbital is a good π acid to stabilize the Ru^0 metal center.

Complexes **6** and **7** crystallized in space groups of orthorhombic *Pnnm* and monoclinic $P2_1/n$, respectively. One-fourth of atoms in the structure of **6** were located from the electron density map, and the complete molecule can be generated from the symmetry operation. The axial nitrato group was disordered in two sites with 50% occupancy for each one. In the structure of **7**, half of the molecule was observed, and the noncoordinated PhSe moiety on *bis*(phenylseleno)-methane was dangling in two positions with a ratio of 4:1 on site-occupancy factors. The molecular diagrams of **6** and **7** are illustrated in Figure 7, and the selected bond lengths and angles are listed in Table 4. With two thiophene moieties in the macrocycle, the core size of S_2TTP is much smaller than that of

dx.doi.org/10.1021/ic200977n | *Inorg. Chem.* 2011, 50, 11947–11957

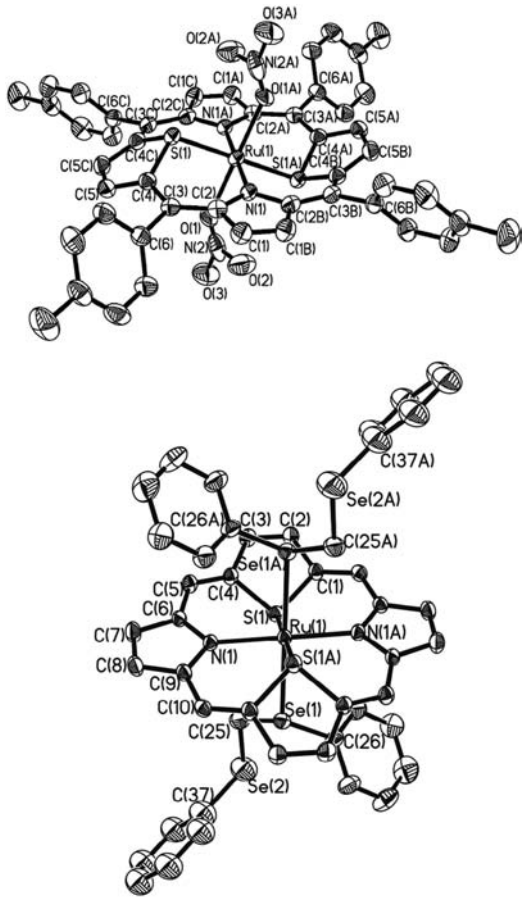

Figure 7. Molecular structures of ruthenium dithiaporphyrin complex **6** (up) and **7** (down, tolyl groups omitted for clarity).

Table 4. Selected Bond Distances and Angles for 6 and 7

	6	7
	bond distances (Å)	
Ru(1)−N(1)	2.069(4)	2.103(4)
Ru(1)−X_{axial}	2.145(4)	2.4935(8)
Ru(1)−S(1)	2.2335(11)	2.2669(16)
	bond angles (deg)	
S(1)−Ru(1)−X_{axial}	90.03(14)	92.56(4)
N(1)−Ru(1)−S(1)	90	90.01(13)
N(1)−Ru(1)−X_{axial}	90	85.79(13)
X_1−Ru(1)−X_2	180	180
Φ^a (deg)^a	17.11(51)	20.02(24)
$\Delta(S)^b$ (Å)	0.84	0.94
Λ^a (deg)	61.86(16)	63.10(18)

^{a}See Table 2 for the define on the angles. ^{b}Deviation of sulfur atom from mean-plane defined by two pyrroles and meso carbons.

STTPH. Therefore, similar to the conformation of Ru(S_2TTP)-Cl_2, both thiophene rings of S_2TTP in **6** and **7** tilted toward opposite directions from the S_2TTP mean plane in order to accommodate the ruthenium ion. The ruthenium centers in both complexes were of six-coordinated octahedral geometry. The Ru−N and Ru−S bond distances of 2.069(4) and 2.2335(11) Å, respectively, for complex **6** were significantly shorter than those of 2.103(4) and 2.2669(16) Å for complex **7**, which indicate the distinctively different oxidation state among two metal centers. The deviation of sulfur atoms from the 14 thiophene-excluded macrocyclic mean planes of dithiaporphyrin was 0.84 Å for **6** and 0.94 Å for **7**, while the bending angles of the thiophene ring were 17.11(51)° in **6** and 20.02(24)° in **7**. Larger deviations and bending angles in **6** and **7** than those of **1**−**5** suggest a larger intrinsic steric constraint in dithiaporphyrin than in thiaporphyrin core. Although the vector connecting two axial coordinating atoms was not perpendicular to the thiophene-excluded dithiaporphyrin mean plane, it was near orthogonal to the line of S(1)−Ru(1)−S(1A) in both **6** and **7**. The nitrato groups in **6** coordinating to the Ru(II) center in a unidentate O-bound coordination mode with a Ru−O distance of 2.145(4) Å are slightly longer than those of **2**. Axial PhSe−CH_2−SePh coordinating to the Ru(0) center was unidentate with Ru−Se distances of 2.4935(8) Å. Intermolecular cross-linking interactions between sulfur atoms were located in the crystal lattices of **6** and **7** to form a one-dimensional linear chain. The intermolecular linear chains pack into a three-dimensional channel-type structure (Figure 8). The dimensions of the

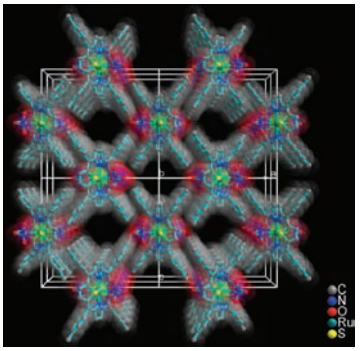

Figure 8. The linear chains packed into channels in the crystal lattice of **6**.

channel in **6** are 9.46 × 9.46 $Å^2$, measured from the distances between two opposite walls constructed by *meso* tolyl groups. With the presence of bulky *bis*(phenylseleno)methane groups on the axial positions, channels in **7** are smaller than those in **6**.

CONCLUSIONS

In this work, the preparations of stable ruthenium thiaporphyrin and dithiaporphyrin complexes have been achieved. The availability of [Ru(STTP)(CO)Cl] and [Ru(S_2TTP)$(Cl)_2$] provides essential starting complexes for further manipulation to explore the coordination chemistry of thiaporphyrin and dithiaporphyrin. Similarly, the stable [Ru(STTP)$(Cl)_2$] can be used as a precursor for the preparation of other Ru(III)−thiaporphyrins. According to the ν(CO) values, the spectrochemical series of electron-donating abilities for the studied ruthenium−carbonyl thiaporphyrins is $Cl^- \sim N_3^- > NO_3^- > NO_2^-$. Exceptionally, the reaction of NaSePh of [Ru(S_2TTP)-Cl_2] in CH_2Cl_2 resulted in the formation of *bis*(phenylseleno)-methane coordinating to a Ru^0 center.

ASSOCIATED CONTENT

Supporting Information

Calculated absorption spectra, computed excited energies, oscillator strengths and electronic transitions configurations, NMR spectra (PDF). Crystallographic information (CIF). This material is available free of charge via the Internet at http://pubs.acs.org.

AUTHOR INFORMATION

Corresponding Author

*Phone: 886-2-27898570. Fax: 886-2-27831237. E-mail: chhung@chem.sinica.edu.tw.

Present Address

⊥Department of Applied Chemistry & Polymer Technology, Delhi Technological University, Shahbad Daulatpur, Delhi, India.

ACKNOWLEDGMENTS

We would like to thank the National Science Council (Taiwan) and Academia Sinica for financial support.

REFERENCES

(1) Nam, W. *Acc. Chem. Res.* **2007**, *40*, 522−531.
(2) Bukowski, M. R.; Koehntop, K. D.; Stubna, A.; Bominaar, E. L.; Halfen, J. A.; Muenck, E.; Nam, W.; Que, L. Jr. *Science* **2005**, *310*, 1000−1002.
(3) Che, C.-M.; Huang, J.-S. *Chem. Commun.* **2009**, 3996−4015.
(4) Jiang, G.; Chen, J.; Thu, H.-Y.; Huang, J.-S.; Zhu, N.; Che, C.-M. *Angew. Chem., Int. Ed.* **2008**, *47*, 6638−6642.
(5) Furuta, H.; Asano, T.; Ogawa, T. *J. Am. Chem. Soc.* **1994**, *116*, 767−768.
(6) Chmielewski, P. J.; Latos-Grazynski, L.; Rachlewicz, K.; Glowiak, T. *Angew. Chem., Int. Ed.* **1994**, *33*, 779−781.
(7) Skonieczny, J.; Latos-Grazynski, L.; Szterenberg, L. *Chem.—Eur. J.* **2008**, *14*, 4861−4874.
(8) Matano, Y.; Nakashima, M.; Nakabuchi, T.; Imahori, H.; Fujishige, S.; Nakano, H. *Org. Lett.* **2008**, *10*, 553−556.
(9) Latos-Grazynski, L.; Lisowski, J.; Olmstead, M. M.; Balch, A. L. *J. Am. Chem. Soc.* **1987**, *109*, 4428−4429.
(10) Ulman, A.; Manassen, J. *J. Am. Chem. Soc.* **1975**, *97*, 6540−6544.
(11) Schmidt, J. A. R.; Lobkovsky, E. B.; Coates, G. W. *J. Am. Chem. Soc.* **2005**, *127*, 11426−11435.
(12) Schmidt, J. A. R.; Mahadevan, V.; Getzler, Y. D. Y. L.; Coates, G. W. *Org. Lett.* **2004**, *6*, 373−376.
(13) Jin, N.; Lahaye, D. E.; Groves, J. T. *Inorg. Chem.* **2010**, *49*, 11516−11524.
(14) Yu, X.-Q.; Huang, J.-S.; Zhou, X.-G.; Che, C.-M. *Org. Lett.* **2000**, *2*, 2233−2236.
(15) Birnbaum, E. R.; Labinger, J. A.; Bercaw, J. E.; Gray, H. B. *Inorg. Chim. Acta* **1998**, *270*, 433−439.
(16) Sharma, P. K.; de Visser, S. P.; Ogliaro, F.; Shaik, S. *J. Am. Chem. Soc.* **2003**, *125*, 2291−2300.
(17) Wang, C.; Shalyaev, K. V.; Bonchio, M.; Carofiglio, T.; Groves, J. T. *Inorg. Chem.* **2006**, *45*, 4769−4782.
(18) Latos-Grazynski, L.; Lisowski, J.; Olmstead, M. M.; Balch, A. L. *Inorg. Chem.* **1989**, *28*, 1183−1188.
(19) Latos-Grazynski, L.; Olmstead, M. M.; Balch, A. L. *Inorg. Chem.* **1989**, *28*, 4065−4066.
(20) Chmielewski, P. J.; LatosGrazynski, L.; Olmstead, M. M.; Balch, A. L. *Chem.—Eur. J.* **1997**, *3*, 268−278.
(21) Tung, J.-Y.; Liau, B.-C.; Elango, S.; Chen, J.-H.; Hsieh, H.-Y.; Liao, F.-L.; Wang, S.-L.; Hwang, L.-P. *Inorg. Chem. Commun.* **2002**, *5*, 150−155.
(22) Latos-Grazynski, L.; Lisowski, J.; Chmielewski, P.; Grzeszczuk, M.; Olmstead, M. M.; Balch, A. L. *Inorg. Chem.* **1994**, *33*, 192−197.
(23) Latos-Grazynski, L.; Lisowski, J.; Olmstead, M. M.; Balch, A. L. *Inorg. Chem.* **1989**, *28*, 3328−3331.
(24) Gebauer, A.; Schmidt, J. A. R.; Arnold, J. *Inorg. Chem.* **2000**, *39*, 3424−3427.
(25) Hung, C.-H.; Ou, C.-K.; Lee, G.-H.; Peng, S.-M. *Inorg. Chem.* **2001**, *40*, 6845−6847.
(26) Sheldrick, G. M. *Acta Crystallogr.* **2008**, *A64*, 112−122.
(27) Sheldrick, G. M. *SADABS*; University of Göttingen: Göttingen, Germany, 1996.
(28) Pople, J. A. et al. Gaussian, Inc.: Wallingford, CT, 2004.
(29) Becke, A. D. *J. Chem. Phys.* **1993**, *98*, 5648−5652.
(30) Becke, A. D. *J. Chem. Phys.* **1993**, *98*, 1372−1377.
(31) Becke, A. D. *Phys. Rev. A* **1988**, *38*, 3098−3100.
(32) Lee, C.; Yang, W.; Parr, R. G. *Phys. Rev. B: Condens. Matter* **1988**, *37*, 785−789.
(33) Hay, P. J.; Wadt, W. R. *J. Chem. Phys.* **1985**, *82*, 299−310.
(34) Wadt, W. R.; Hay, P. J. *J. Chem. Phys.* **1985**, *82*, 284−298.
(35) Tomasi, J.; Mennucci, B.; Cammi, R. *Chem. Rev.* **2005**, *105*, 2999−3093.
(36) Zhou, Z.; Cao, C.; Liu, Q.; Jiang, R. *Org. Lett.* **2010**, *12*, 1780−1783.
(37) Allen, F. H. *Acta Crystallogr., Sect. B* **2002**, *58*, 380−388.
(38) Bohle, D. S.; Hung, C.-H.; Smith, B. D. *Inorg. Chem.* **1998**, *37*, 5798−5806.
(39) Addison, C. C.; Logan, N.; Wallwork, S. C.; Garner, C. D. *Quart. Rev., Chem. Soc.* **1971**, *25*, 289−322.
(40) Nakamoto, K. *Infrared and Raman Spectra of Inorganic and Coordination Compounds, Part B: Applications in Coordination, Organometallic, and Bioinorganic Chemistry*; 5th ed.; John Wiley & Sons, Inc.: Hoboken, NJ, 1997.
(41) Nasri, H.; Wang, Y.; Huynh Boi, H.; Scheidt, W. R. *J. Am. Chem. Soc.* **1991**, *113*, 717−719.
(42) Nasri, H.; Ellison, M. K.; Krebs, C.; Huynh, B. H.; Scheidt, W. R. *J. Am. Chem. Soc.* **2000**, *122*, 10795−10804.
(43) Sievertsen, S.; Weidemann, M.; Huckstadt, H.; Homborg, H. *J. Porphyr. Phthalo.* **1997**, *1*, 379−384.
(44) Mukaida, M.; Sato, Y.; Kato, H.; Mori, M.; Ooyama, D.; Nagao, H.; Howell, F. S. *Bull. Chem. Soc. Jpn.* **2000**, *73*, 85−95.
(45) Lisowski, J.; Grzeszczuk, M.; Latos-Grazynski, L. *Inorg. Chim. Acta* **1989**, *161*, 153−163.